Good practice report

Masaru Matsuo*, Rong Zhang and Yuezhen Bin

An understandable approach to the temperature dependence of electric properties of polymer-filler composites using elementary quantum mechanics

https://doi.org/10.1515/cti-2020-0014
Received June 26, 2020; accepted May 3, 2021; published online May 31, 2021

Abstract: In today's society, with a high percentage of elderly people, floor heating to ensure constant temperature and heat jackets in winter play important roles in winter to them to live comfortable lives without compromising health – except tropical zones. Under floor heating maintains a comfortable temperature in a room without polluting the air and heat jackets allow for light clothing at comfortable temperatures. The two facilities are attributed to Joule heat generated by tunnel currents between adjacent short carbon fillers in flexible polymer matrixes under low voltage. The current between adjacent conductive fillers is due to electron transfer associated with elementary quantum mechanics. Most of undergraduate students investigating polymer physics will have learned about electron transfer in relation to the temperature dependence of the conductivity of conductive filler-insulator polymer composites as well as the phenomenon of Joule heat at high school. Despite their industrial importance, most students show little interest for investigating electric properties, since most of polymers are insulation materials. Polymer scientists have carried out qualitative analyses for tunneling current using well-known simplified equations derived from complicated mathematical process formulated by solid-state physicists. Hence this paper is focused on a teaching approach for temperature dependence on electric properties of the polymer-filler composites relating to tunnel current in terms of elementary quantum mechanics. The approach also attempts to bridge education and research by including reference to the application limit of the well-known theories to such complicated composite systems that fillers are dispersed uniformly in the polymer matrix.

Keywords: electric properties; elementary quantum mechanics; polymer composites.

Introduction

Most polymers are insulation materials that are easy to mold. Mixing conductive fillers into polymer matrix provides the temperature dependent conductive property by generation of Joule heat. Joule heat has been applied to home appliances such as electric oven, electrical cooking plates and induction cooking. This paper deals with a teaching process for the electric properties of polymer-filler composites built on knowledge acquired at high school in an attempt to get undergraduate and/or graduate students interested in talking in class.

***Corresponding author: Masaru Matsuo**, Department of Polymer Science and Materials, Dalian University of Technology, Dalian 116024, China, E-mail: mm-matsuo@live.jp
Rong Zhang, Hubei Provincial Key Laboratory of Green Materials for Light Industry, Hubei University of Technology, Wuhan 430068, China, E-mail: zhangrong@hbut.edu.cn
Yuezhen Bin, Department of Polymer Science and Materials, Dalian University of Technology, Dalian 116024, China, E-mail: binyz@dlut.edu.cn

Now, let's briefly review of Joule heat as taught in high school.

The generation of Joule heat is represented as a model in Figure 1 by the movement of free electrons in a conductor with cross section S [m^2] and length ℓ [m], in which n is the number of free electrons in a unit volume and u is the average velocity under applied voltage V. Free electrons accelerate in an electric field but their velocity decreases, when they collide with positive ions, and then their final velocity become constant. This indicates the constant kinetic energy is consumed as Joule heat is used to generate the vibration of positive ions.

$$Q = \text{power} \times \text{distance} \times \text{total number of free electrons} = e\frac{V}{\ell} \times ut \times n\ell S = enuS \times Vt = I \times Vt$$
$$= IVt \ (I : \text{electric current}) \tag{1}$$

$Q = IVt$ is also given as $Q = IVt = I^2Rt$ using Ohm's law ($V = RI$).

However, composites utilized in floor heating and heat jackets have conductive fillers dispersed uniformly in a flexible insulating polymer matrix (Bin, Chen, Tashiro, & Matsuo, 2008; Isaji, Bin, & Matsuo, 2009; Koganemaru, Bin, Agari, & Matsuo, 2004; Xi, Ishikawa, Bin, & Matsuo, 2004). These composites are called as positive temperature coefficient (PTC) materials and are associated with thermal volume expansion as temperatures increase. As an example, the floor heating plate is shown in Figure 2. This method of heating plays an important role in avoiding the emission of carbon dioxide in comparison with gas water heating.

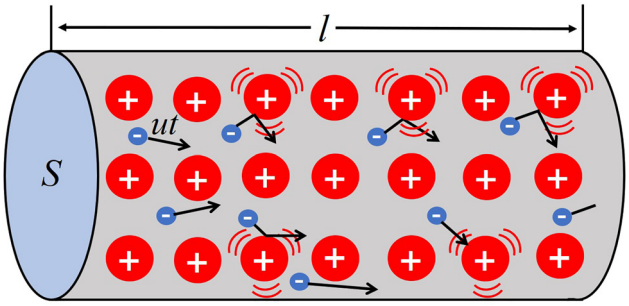

Figure 1: A model of the movement of free electrons in conductor.

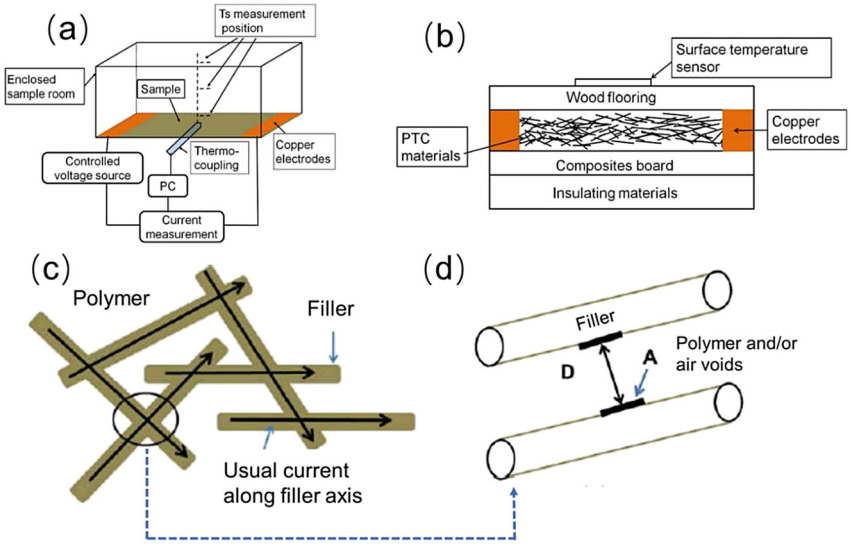

Figure 2: (a) Sketch in a room with floor heating function. (b) Cross section of PTC plate. (c) Short fillers overlapped in polymer matrix. (d) Enlargement of overlapped position between adjacent fillers in (c).

In PTC materials associated with electric current generated by eletron transfer, as shown in Figure 2d, D is the average gap distance between adjacent fillers to allow electron transfer and A is the area over which most of the tunneling occurs. The average means that there exist many gaps with small fluctuations in the effective distance range in the composite. In this case, D in Figure 2d means the average distance associated with effective tunneling.

On elevating temperature of PTC materials beyond the setting range, the electricity is cut off automatically by thermal expansion of matrix leading to excess Joule heat, while it flows again by the matrix shrinkage accompanying cooling. Certainly, the PTC mechanism is well-known function associated with tunnel current.

To facilitate a systematic understanding of the temperature dependence of tunnel current, for students, the detailed explanation for tunnel current density must be described in terms of important three factors, the permeability coefficient induced by the WKB (Wentzel Kramers Brillouin) approximation, the Fermi distribution function, and the thermal fluctuation probability. Of the three, the students are not likely to be familiar to the WKB approximation, and so the detailed explanation must be explained in combination with tunnel current density. Reported tunnel current theories (Fowler & Nordheim, 1928; Gossling, 1926; Millikan & Eyring, 1926; Nordheim, 1928; Schottky, 1923; Simmons, 1963) were constructed for an ideal system where a very thin flat insulating film is sandwiched between two metal electrodes, while more recent theory has an ideal tunnel junction being a parallel-plate capacitor with distance d (w in Ref. Sheng, 1980) and area A. Namely, the theory is based on an ideal system where current can flow, by the tunnel effect, between the parallel-plates with constant d and A values, so that the parallel-plates correspond to two electrodes.

However, the application of the theories to the complicated systems, i.e. the conductive fillers dispersed in an insulation matrix, only applies to the limited number of systems that have resistivity between the adjacent fillers much higher than the interface resistivity between the bulk and the electrode and the resistivity for carrier movement within the fillers. This is the most important subject, although most of papers by polymer scientists have never referred to the limit, since the interface resistivity between bulk and electrode and the filler resistivity by carrier movement within fillers are out of the framework discussed for ideal systems. The reasons for this are referred to in detail in Sections "*Thermal fluctuation-induced tunneling effect*" and "*Application limit of tunnel current theory to polymer-filler composite*".

This paper is written as an understandable text for the electric property of polymer-filler composites associated with elementary quantum mechanics in terms of aspects of education. Hence most of mathematical evaluations concerning tunnel effects are described in Supplementary material (I–V). Supplementary material in this paper is not a mere supplement but is written as a commentary text for polymer scientists who are not familiar with mathematics. Of course, the fundamental knowledge about quantum mechanics has been in the spotlight in recent quantum technology fields.

Simple application of Schrödinger equation to tunnel effect

This section refers to the one-dimensional Schrödinger wave function built on basic knowledge of mathematics at the high school level, which is enough for teaching the tunnel effect.

Generally, wave function Ψ with wavelength λ is represented as a trigonometric function. Traveling wave to right with velocity u moves ut in the x direction (one dimensional case) after time t.

$$\Psi = A \sin \frac{2\pi}{\lambda} (x - ut) = A \sin 2\pi (kx - \nu t) \tag{2}$$

where $k = 1/\lambda$ and $\nu = u/\lambda$ (ν: frequency)

Equation (2) is one of the solutions of the following differential equation:

$$\frac{\partial^2\Psi}{\partial x^2} = \frac{1}{u^2}\frac{\partial^2\Psi}{\partial t^2} \tag{3}$$

In addition to Eq. (2), Eq. (4) provides another solution of Eq. (3) as follows:

$$\Psi = A\cos 2\pi(kx - \nu t) \tag{4}$$

Accordingly, the solution of Eq. (3) is given by

$$\Psi = A\cos 2\pi(kx - \nu t) + iA\sin 2\pi(kx - \nu t) = A\exp[2\pi i(kx - \nu t)] \tag{5}$$

Equation (5) can be applied to the representation of the de Broglie wave but it is independent of wave-particle duality.

To combine the relationship between particle and wave properties, the following replacement for energy E and wave number k must be adopted:

$$E = h\nu, k = \frac{1}{\lambda} = \frac{p}{h}\ (\lambda = h/mu = h/p) \tag{6}$$

where h is Planck's constant, p is momentum, and m is mass of a quantum particle.

Hence, Eq. (5) can be replaced as

$$\Psi = A\exp\left[\frac{2\pi i}{h}(px - Et)\right] \tag{7}$$

Equation (7) contains both properties of particles and waves.

By using the simple mathematical treatments represented in Supplementary material I, the Schrödinger wave function is rewritten as

$$\frac{d^2}{dx^2}\varphi(x) = \frac{8\pi^2 m(U(x) - E)}{h^2}\varphi(x) = p^2\varphi(x) \tag{8}$$

where $U(x)$ and E are potential energy and the total energy, respectively.

The wave function $\varphi(x)$ is replaced by assuming the phase $S(x)$ as follows:

$$\varphi(x) = \exp\left[\frac{2\pi i}{h}S(x)\right] \tag{9}$$

Now, let's consider the tunnel effect by using the Schrödinger wave function, when $U(x)$ is given by rectangular potential U_o independent of x as shown in Figure 3.

Based on Eq. (8), wave functions $\varphi(x)$ at Regions *I*, *II*, and *III* in Figure 3 can be written as follows:

$$\frac{d^2}{dx^2}\varphi(x) = -\frac{8\pi^2 mE}{h^2}\varphi_I(x) = -k^2\varphi_I(x) \quad \left(k = \frac{2\pi}{h}\sqrt{2mE}\right) \tag{8-1}'$$

$$\frac{d^2}{dx^2}\varphi_{II}(x) = \frac{8\pi^2 m(U_o - E)}{h^2}\varphi_{II}(x) = \rho^2\varphi_{II}(x) \quad \left(\rho = \frac{2\pi}{h}\sqrt{2m(U_o - E)}\right) \tag{8-2}'$$

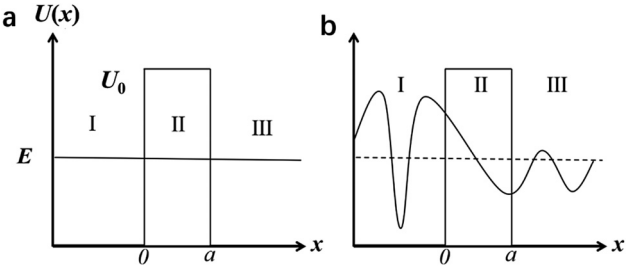

Figure 3: Transmission of electron with energy E across rectangular potential U_o.
(a) The relationship between E and U_o. (b) Wave functions at Regions I, II and III.

$$\frac{d^2}{dx^2}\varphi_{III}(x) = -\frac{8\pi^2 mE}{h^2}\varphi_{III}(x) = -k^2\varphi_{III}(x) \quad \left(k = \frac{2\pi}{h}\sqrt{2mE}\right) \tag{8-3)'}$$

At Region I, the traveling wave along the x axis must consider the reflection wave by collision at potential barrier U_o, while at Region *III*, only traveling waves going through Region *II* exist. Accordingly, the above three equations can be written as

$$\varphi_I(x) = A\exp(ikx) + B\exp(-ikx) \qquad x \le 0 \tag{10-1}$$

$$\varphi_{II}(x) = C\exp(\rho x) + D\exp(-\rho x) \qquad 0 \le x \le a \tag{10-2}$$

$$\varphi_{III}(x) = F\exp(ikx) \qquad a \ge x \tag{10-3}$$

The wave functions must be connected smoothly at each boundary of the regions. Thus, the following relations must be satisfied.

$$\varphi_I(0) = \varphi_{II}(0) \rightarrow A + B = C + D \tag{11-1}$$

$$\frac{d}{dx}\varphi_I(0) = \frac{d}{dx}\varphi_{II}(0) \rightarrow ik(A - B) = \rho(C - D) \tag{11-2}$$

$$\varphi_{II}(a) = \varphi_{III}(a) \rightarrow C\exp(\rho a) + D\exp(-i\rho a) = F\exp(ika) \tag{11-3}$$

$$\frac{d}{dx}\varphi_{II}(a) = \frac{d}{dx}\varphi_{III}(a) \rightarrow \rho\{C\exp(\rho a) - D\exp(-\rho a)\} = ikF\exp(ika) \tag{11-4}$$

Among the unknown five parameters (A, B, C, D, F), the necessary parameters A, B, *and* F in Eq. (11) can be described as following relationships.

$$\frac{F}{A} = \frac{4ik\rho\exp(-ika)}{\left[(\rho + ik)^2\exp(-\rho a) - (\rho - ik)^2\exp(\rho a)\right]} \tag{12-1}$$

and

$$\frac{B}{A} = \frac{\left(k^2 + \rho^2\right)[\exp(\rho a) - \exp(-\rho a)]}{\left[(\rho + ik)^2\exp(-\rho a) - (\rho - ik)^2\exp(\rho a)\right]} \tag{12-2}$$

By considering the positive direction of the waves along the x direction, each flow of possibility of the incident, reflection and transmitted waves are given by Eqs. (13), (14) and (15), respectively.

$$J_{in} = \frac{h}{2\pi i}\frac{1}{2m}\left[\varphi_{in}(x)\frac{d\varphi_{in}^*(x)}{dx} - \frac{d\varphi_{in}(x)}{dx}\varphi_{in}^*\right] = \frac{hk}{2\pi m}|A|^2 \tag{13}$$

$$J_{ref} = \frac{h}{2\pi i}\frac{1}{2m}\left[\varphi_{ref}(x)\frac{d\varphi_{ref}^*(x)}{dx} - \frac{d\varphi_{ref}(x)}{dx}\varphi_{ref}^*\right] = \frac{-hk}{2\pi m}|B|^2 \tag{14}$$

$$J_{trans} = \frac{h}{2\pi i}\frac{1}{2m}\left[\varphi_{trans}(x)\frac{d\varphi_{trans}^*(x)}{dx} - \frac{d\varphi_{trans}(x)}{dx}\varphi_{trans}^*\right] = \frac{hk}{2\pi m}|F|^2 \tag{15}$$

Accordingly, transmittance (T) and reflectivity (R) are given by

$$T = \frac{J_{trans}}{J_{in}} = \frac{|F|^2}{|A^2|} = \frac{1}{1 + \frac{U_o^2}{4E(U_o - E)}\sin h^2\left(\frac{2\pi a}{h}\sqrt{2m(U_o - E)}\right)} \tag{16}$$

and

$$R = \frac{J_{ref}}{J_{in}} = \frac{|B|^2}{|A|^2} = \frac{\frac{U_o^2}{4E(U_o-E)} \sin h^2\left(\frac{2\pi a}{h}\sqrt{2m(U_o-E)}\right)}{1+\frac{U_o^2}{4E(U_o-E)} \sin h^2\left(\frac{2\pi a}{h}\sqrt{2m(U_o-E)}\right)} \tag{17}$$

Hence, $T + R = 1$.

Equation (16) has been used for teaching tunnel current for the undergraduate students of electric department but it has been out of the frame for most of the graduate students of the polymer department. Then, let's try exercise.

Exercise

(Question)

Put a particle as an electron with kinetic energy $E = 9.00$ eV in one dimensional box with barrier height of $U_o = 10$ eV and barrier of 10 Å (1 nm) and calculate the electron transmittance by using Eq. (16). Incidentally, $(U_o - E) = 1\ \text{eV} = 1.602 \times 10^{-12}$ erg, $a = 10\ \text{Å} = 1\ \text{nm} = 10^{-7}$ cm, $m = 9.109 \times 10^{-28}$ g, $h = 6.625 \times 10^{-27}$ erg · sec.

(Answer)

$$\sinh^2(p\alpha) = \sinh^2\left(\frac{2\pi a}{h}\sqrt{2m(V_o-E)}\right) = \frac{\exp(2\rho a) + \exp(-2\rho a) - 2}{4} = 7014.39$$

Thus, $T = 5.1320 \times 10^{-5}$ and $R = 0.99995$.

Incidentally, $T = 6.1821 \times 10^{-3}$ and $R = 0.99382$ at $U_o = 10$ eV and $E = 9.90$ eV.

The two values for T mean that the transmittance increases with decreasing the difference $(U_o - E)$ between potential barrier and kinetic energy.

Additionally, in the case of $E > U_o$, classical theory provides $T = 1$ and $R = 0$, but quantum mechanics provides the following results.

$$T = \frac{1}{1+\frac{U_o^2}{4E(E-U_o)}\sin^2\left(\frac{2\pi a}{h}\sqrt{2m(E-U_o)}\right)} \tag{18}$$

and

$$R == \frac{\frac{U_o^2}{4E(E-U_o)}\sin^2\left(\frac{2\pi a}{h}\sqrt{2m(E-U_o)}\right)}{1+\frac{U_o^2}{4E(E-U_o)}\sin^2\left(\frac{2\pi a}{h}\sqrt{2m(E-U_o)}\right)} \tag{19}$$

At $E = 10.00$ eV, $U_o = 9$ eV, and $a = 10\ \text{Å} = 1\ \text{nm} = 10^{-7}$cm, T and R are given by

$T = 0.9841$ and $R = 0.0159$

This indicates that T is not always unity even at $E > V_o$. However, it should be noted that T becomes unity and $R = 0$ at $2\pi\sqrt{2m(E-U_o)}a/h = n\pi$ ($n = 1, 2, 3, ———$), periodically.

Namely,

$$E = E_n \equiv U_o + \frac{h^2 n^2}{8ma^2} \tag{20}$$

Such property is termed resonant transmission.

Analysis for tunnel effect using the WKB approximation

The general transmittance T is given in a complicated form using integration, in many technical textbooks. This section explains the process in detail together with Supplementary material II. Different from the rectangle in

Figure 3, the potential $U(x)$ for the tunnel effect is generally given by an arbitrary function as shown in Figure 4a. This model has been adopted to explain the tunnel effect of electrons.

When a particle (electron) with energy E can enter in the positive direction along x-axis from Region I ($x < a$), the particle at Region III ($x > b$) provides the traveling wave in the positive direction along the x axis. The turning points of classical mechanism are $x = a$ and $x = b$ satisfying $E = U(a) = U(b)$. This concept is the same as that in Figure 3. However, $U(x)$ is not a simple function and the boundary condition is also not simple like Eq. (11).

Substituting Eq. (9) into Eq. (8) and carrying out the second derivatives, we have

$$-\frac{h^2}{8\pi^2 m}\frac{d^2}{dx^2}e^{\frac{2\pi S(x)}{h}i} = -\frac{h^2}{8\pi^2 m}\frac{d}{dx}\left[\frac{2\pi i}{h}\frac{dS(x)}{dx}e^{\frac{2\pi S(x)}{h}i}\right]$$

$$= -\frac{h^2}{8\pi^2 m}\left[\left(\frac{2\pi i}{h}\frac{dS(x)}{dx}\right)^2 + \frac{2\pi i}{h}\frac{d^2S(x)}{dx^2}\right]e^{\frac{2\pi S(x)}{h}i}$$

Hence Eq. (8) can be written as follows:

$$\frac{1}{2m}\left(S'(x)^2 - \frac{hS''(x)}{2\pi}i\right) + U(x) = E \tag{21}$$

Assuming $[S'(x)]^2 >> (h/2\pi)S''(x)$, Eq. (21) becomes Hamilton–Jacobi equation.

Now, let's try perturbation series expansion of S (abbreviation of $S(x)$) by $h/2\pi$ as follows:

$$S = S_o + \frac{h}{2\pi}S_1 + \left(\frac{h}{2\pi}\right)^2 S_2 + - - - - - \tag{22}$$

This method is termed as the WKB approximation.

Substituting Eq. (22) into Eq. (21) and collecting in h order, Eq. (21) is written by

$$\frac{1}{2m}\left[S_o'^2 + \frac{h}{2\pi}(2S_o'S_1' - iS_o'') - - - -\right] + U(x) - E = 0 \tag{23}$$

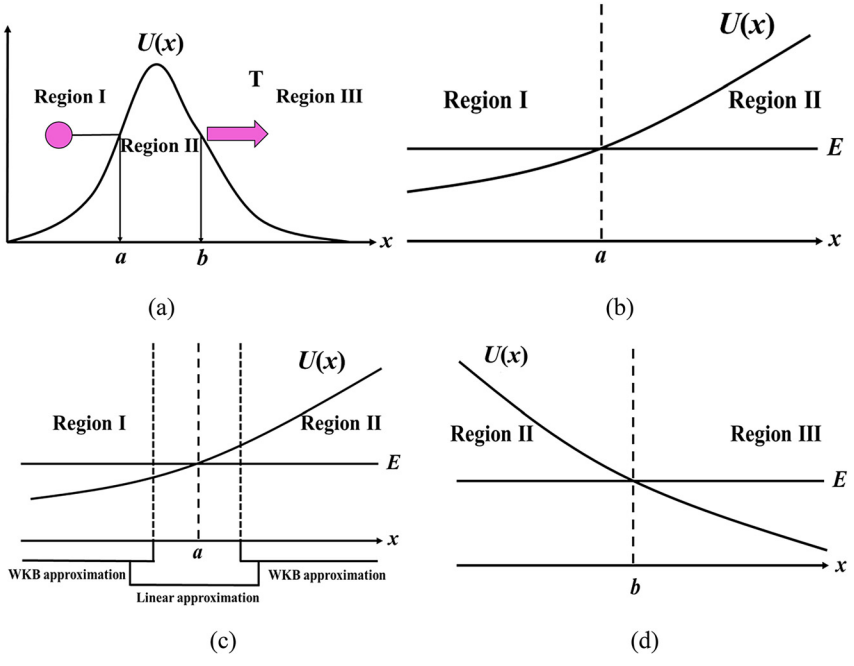

Figure 4: (a) Transmission of electron with energy E across arbitrary potential function $U(x)$ at turning points a and b. (b) Potential around turning point a. (c) Linear approximation around turning point a. (d) Potential around turning point b.

Neglecting terms beyond h^2 order, the following relationships can be obtained.

$$S_o'^2 = 2m(E - U(x)) \ \ 0 - \text{order} \tag{24-1}$$

$$S_1' = \frac{iS_o''}{2S_o'} \ \ 1\text{st} - \text{order} \tag{24-2}$$

The WKB approximation treats the first order of h, and then it terms as quasi-classical approximation. Incidentally, S has the meaning of action integral at $h \to 0$ indicating the transfer from quantum mechanics to classical mechanics. By using the WKB approximation, two approximate solutions can be proposed. One is the approximate solution at the reachable area of the particle by classical mechanics. The other is the approximate solution at the unreachable area of the particle in terms of classical mechanics but it becomes the approximate solution at the reachable area of the particle by the tunnel effect in terms of quantum mechanics. In the latter case, it is necessary to connect singularity termed as turning points separating the two areas and the connecting method is established by a somewhat complicated procedure using the Airy function, which is described in Supplementary material II.

Now, we shall consider electron movement with potential barrier $U(x)$ (Region I) in Figure 4b, in which the potential $U(x)$ shows right upward curve with increasing x.

At $E > U(x)$ (Region I), electron transfer can be analyzed by classical theory of physics.

Then the local momentum $p(x)$ at $E > U(x)$ is given as follows:

$$p(x) = \frac{2\pi}{h}\sqrt{2m(E - U(x))} \tag{25}$$

The above condition corresponds to the possible region of classical mechanics of particles (electrons).

By substituting Eq. (25) into Eq. (24-1),

$$S_o' = \frac{dS_o}{dx} = \pm\frac{h}{2\pi}p(x) \to S_o(x) = \pm\frac{h}{2\pi}\int_a^x p(x')dx' \tag{26}$$

By substituting Eq. (25) into Eq. (24-2) and carrying out the integration,

$$S_1' = \frac{dS_1}{dx} = \frac{ip'(x)}{2p(x)} \to S_1(x) = \frac{i}{2}\ell np(x) \tag{27}$$

By substituting Eqs. (26) and (27) into Eq. (9), the right part of Eq. (9) is given by

$$\exp\left[\frac{2\pi i}{h}\left(S_o + \frac{h}{2\pi}S_1\right)\right] = \exp\left[\pm\frac{2\pi i}{h}\int_a^x p(x')dx - \frac{1}{2}\ell np(x)\right] = \frac{1}{\sqrt{p(x)}}\exp\left[\pm\frac{2\pi i}{h}\int_a^x p(x')dx'\right]$$

Hence the general wave function $\varphi(x)$ can be given by a linear combination of the two independent solutions as follows:

$$\varphi(x) = \frac{C_+}{\sqrt{p(x)}}\exp\left[\frac{2\pi i}{h}\int_a^x p(x')dx'\right] + \frac{C_-}{\sqrt{p(x)}}\exp\left[-\frac{2\pi i}{h}\int_a^x p(x')dx'\right] \tag{28}$$

where C_+ and C_- are constant integrations. To simplify the representation, $(2\pi/h)\int_a^x p(x')dx'$ is rewritten as

$$\eta(x,a) = \int_x^a \frac{2\pi\sqrt{2m(E - U(x'))}}{h}dx' = -\eta(a,x) = -\int_a^x \frac{2\pi\sqrt{2m(E - U(x'))}}{h}dx' \tag{29}$$

Thus, in Region I, the wave function obtained using the WKB approximation is given by

$$\varphi_1(x) = \frac{C_+}{\sqrt{p(x)}}\exp[-i\eta(x,a)] + \frac{C_-}{\sqrt{p(x)}}\exp[i\eta(x,a)] \ (x < a) \tag{30}$$

$\eta(x,a)$ is the phase measured from turning point a, which is termed a local phase. Since $\eta(x,a) \geq 0$, $\eta(x,a)$ becomes larger as x becomes far from the turning point a. Accordingly, the first and second terms of Eq. (30) represent the waves along the positive and negative directions, respectively. This means that existence

probability of a particle between x and $x + dx$ is $|\varphi(x)|^2$ and the probability is proportional to $1/p(x)$, which indicates the inversed proportion to the local momentum.

When $E < U(x)$ (Region II), the electron transfer is out of the framework of classical analysis. The local momentum is defined by

$$\rho(x) = \frac{2\pi}{h}\sqrt{2m(U(x) - E)} \tag{31}$$

Of course, $|\rho(x)| = |p(x)|$.

By using a method similar to $p(x)$ in Eqs. (26) and (27), the application to $\rho(x)$, provides

$$S_o' = \frac{dS_o}{dx} = \pm i\frac{h}{2\pi}\rho(x) \rightarrow S_o(x) = \pm i\frac{h}{2\pi}\int_a^x \rho(x')dx' \tag{32}$$

and

$$S_1' = \frac{dS_1}{dx} = \frac{i\rho'(x)}{2\rho(x)} \rightarrow S_1(x) = \frac{i}{2}\ell n\rho(x) \tag{33}$$

Similarly, the general wave function $\varphi(x)$ can be given by a linear combination of the two independent solutions as follows:

$$\varphi(x) = \frac{D_+}{\sqrt{\rho(x)}}\exp\left[\frac{2\pi}{h}\int_a^x \rho(x')dx'\right] + \frac{D_-}{\sqrt{\rho(x)}}\exp\left[-\frac{2\pi}{h}\int_a^x \rho(x')dx'\right] \tag{34}$$

The first and seconds terms in Eq. (34) represent the waves along the positive and negative directions, respectively. Following Eq. (29), Eq. (34) is represented by

$$\varphi_2(x) = \frac{D_+}{\sqrt{\rho(x)}}\exp[\eta(a,x)] + \frac{D_-}{\sqrt{\rho(x)}}\exp[-\eta(a,x)] \ (x > a) \tag{35}$$

It should be noted that the solutions of wave function in Region I and that in Region II must be connected at the turning point a. However, the solutions using the WKB approximation are not consistent at the turning point a. The diagram allowing the WKB approximation for dull potential is shown in Figure 4c.

Hence the exact solutions must be obtained at the region close to $x = a$. The potential $U(x)$ in the vicinity of the turning point a, can be approximated linearly and the exact solution can be obtained. The two wave functions, Eqs. (30) and (35), can be connected by using the coefficients of the WKB approximation in Region I and Region II. The detailed procedure by using the Airy function is described as Eqs. (SII-1)–(SII-25) in Supplementary material II. The result is as follows:

$$C_\pm = \left(\frac{1}{2}D_+ \pm iD_-\right)\exp\left(\mp\frac{i\pi}{4}\right) \tag{36}$$

On replacing C_+ and C_- by D_+ and D_-, $\varphi_1(x)$ is rewritten by

$$\varphi_1(x) = \frac{D_+}{\sqrt{p(x)}}\cos\left[\eta(x,a) + \frac{\pi}{4}\right] + \frac{2D_-}{\sqrt{p(x)}}\sin\left[\eta(x,a) + \frac{\pi}{4}\right] \tag{37}$$

$\varphi_1(x)$, which is represented by Eq. (37), is the WKB approximation solution in Region I which is in connection with the solution of $\varphi_2(x)$ in Region II.

Incidentally, as described for Eq. (21), the absolute value of the second term must be much smaller than that of the first term on adopting the WKB approximation. $[S'(x)]^2 >> (h/2\pi)S''(x)$. Then,

$$\frac{h}{2\pi}|S''| << |S'^2| \rightarrow \left|\frac{d}{dx}\left(\frac{h}{2\pi S'}\right)\right| << 1 \rightarrow \left|\frac{d}{dx}\left(\frac{1}{p(x)}\right)\right| << 1$$

By using the de Broglie wavelength $\lambda(x) = 2\pi/p(x)$, the above condition can be satisfied at $(1/2\pi)|d\lambda(x)/dx| << 1$. This indicates that the WKB approximation can be established when the fluctuation of the de Broglie wavelength is negligibly small on transferring the distance $\lambda(x)$.

In the region of $a < x < b$, the following relationship can be obtained.

$$\eta(a,x) = \eta(a,b) + \eta(b,x) = P + \eta(b,x) \tag{38}$$

where

$$P = \eta(a,b) = \int_a^b \frac{2\pi\sqrt{2m(U(x)-E)}}{h}dx \tag{39}$$

By using Eq. (39), Eq. (37) can be written as follows: (see Eq. (SII-25))

$$\begin{aligned}\varphi_2(x) &= \frac{D_+}{\sqrt{\rho(x)}}\exp[\eta(a,x)] + \frac{D_-}{\sqrt{\rho(x)}}\exp[-\eta(a,x)] \\ &= \frac{C}{\sqrt{\rho(x)}}\left\{\exp\left[-\eta(b,x) - \frac{i\pi}{4}\right] + \frac{1}{2}\exp\left[\eta(b,x) + \frac{i\pi}{4}\right]\right\}\end{aligned} \tag{40}$$

where

$$D_+ = \frac{1}{2}C\exp\left[-P + \frac{i\pi}{4}\right] \tag{41-1}$$

$$D_- = C\exp\left[P - \frac{i\pi}{4}\right] \tag{41-2}$$

By using Eq. (36),

$$C_+ = C\left[\exp(P) + \frac{1}{4}\exp(-P)\right] \tag{42-1}$$

$$C_- = -iC\left[\exp(P) - \frac{1}{4}\exp(-P)\right] \tag{42-2}$$

As for the $U(x)$ with downward-sloping curve in Figure 4d, the wave functions $\varphi(x)$ can be obtained by using the method similar to the up-sloping curve in Figure 4b.

That is, the wave functions must be obtained at $x > b$ ($U(x) < E$, Region III) and $x < b$ ($U(x) > E$, Region II), when the turning point is defined as b. To connect the solutions of the WKB approximation in the two regions II and III, the potential $U(x)$ in the vicinity of the turning point b, can be approximated linearly and the exact solution can be obtained by the method similar to Figure 4c.

The mathematical treatment using the Airy function is somewhat complicated and the concrete mathematical procedure is described in Supplementary material II.

By using the above method discussed for Regions I and II, the wave functions $\varphi_2(x)$ and $\varphi_3(x)$ of Regions II and III are given by

$$\varphi_2(x) = \frac{A_+}{\sqrt{\rho(x)}}\exp[\eta(x,b)] + \frac{A_-}{\sqrt{\rho(x)}}\exp[-\eta(x,b)] \tag{43}$$

and

$$\varphi_3(x) = \frac{B_+}{\sqrt{p(x)}}\exp[\eta(b,x)] + \frac{B_-}{\sqrt{p(x)}}\exp[-\eta(b,x)] \tag{44}$$

Here it should be noted that Eq. (43) is the same as Eq. (35) but is written differently to easily connect of the wave functions of Regions II and III at the turning point b.

As discussed already, for Regions I and II, the above two wave functions must be connected. The detailed treatment is described in Eqs. (SII-26)–(SII-40). Incidentally, only the traveling wave going through Region II exists at $x > b$. Then, $B_- = 0$.

$$\varphi_3(x) = \frac{B_+}{\sqrt{p(x)}} \exp[\eta(b,x)] \tag{45}$$

Following Supplementary material II, the result is given by

$$B_+ = \left(\frac{1}{2}A_+ - iA_-\right)\exp\left(+\frac{i\pi}{4}\right) \tag{46}$$

Through complicated treatments represented in Supplementary material II, the wave functions, $\varphi_I(x)$ (Region I), $\varphi_{II}(x)$ (Region II) and $\varphi_{III}(x)$ (Region III) are described as Eqs. (SII-20), (SII-25), and (SII-40), respectively. The three equations are summarized as follows:

$$\begin{aligned}\varphi_I(x) &= \frac{1}{\sqrt{p(x)}}\{C_+\exp[-i\eta(x,a)] + C_-\exp[i\eta(x,a)]\} \\ &= \frac{1}{\sqrt{p(x)}}\{C_+\exp[i\eta(a,x)] + C_-\exp[-i\eta(a,x)]\}\; x < a\end{aligned} \tag{47}$$

$$\varphi_{II}(x) = \frac{C}{\sqrt{\rho(x)}}\left\{\exp\left(-\eta(b,x) - \frac{i\pi}{4}\right) + \frac{1}{2}\exp\left(\eta(b,x) + \frac{i\pi}{4}\right)\right\}\; a < x < b \tag{48}$$

$$\varphi_{III} = \frac{C}{\sqrt{p(x)}}\exp(i\eta(b,x))\; x > b \tag{49}$$

where

$$C_+ = C\left\{\exp(P) + \frac{1}{4}\exp(-P)\right\} \tag{42-1a}$$

$$C_- = -iC\left\{\exp(P) - \frac{1}{4}\exp(-P)\right\} \tag{42-2b}$$

P is given by Eq. (39) and the following relationship can be given by

$$\eta(b,x) = \eta(b,a) + \eta(a,x) = -\eta(a,b) + \eta(a,x) = -P + \eta(a,x) \tag{50}$$

Accordingly, the flow of possibility J_I of the incident wave is calculated by using the incident wave function as follows:

$$\varphi_{in}(x) = \left(\frac{C_+}{\sqrt{p(x)}}\right)\exp(i\eta(a,x)). \tag{51}$$

$$\begin{aligned}J_I &= \frac{h}{2\pi i}\frac{1}{2m}\left[\varphi_{in}(x)\frac{d\varphi_{in}^*(x)}{dx} - \frac{d\varphi_{in}(x)}{dx}\varphi_{in}^*\right] \\ &= \frac{h}{2\pi m}\frac{|C_+|^2}{p(x)}\frac{d\eta(a,x)}{dx} = \frac{h}{2\pi m}|C_+|^2 = \frac{h}{2\pi m}\left(\exp(\eta(a,b) + \frac{1}{4}\exp(-\eta(a,b))\right)^2|C|^2\end{aligned} \tag{52}$$

where

$$\eta(a,x) = \int_a^x p(x')dx' \rightarrow \frac{d\eta(a,x)}{dx} = p(x) \tag{53}$$

As for the transmitted wave function given by Eq. (49), the flow of possibility J_T is given by using the treatment similar to the incident wave.

$$J_T = \frac{h}{2\pi m}|C|^2 \tag{54}$$

Accordingly, the permeability coefficient is given by

$$T = \frac{|J_T|}{|J_I|} = \frac{\exp(-2\eta(a,b))}{\left(1+\frac{\exp(-2\eta(a,b))}{4}\right)^2} \tag{55}$$

The WKB approximation can be constructed favorably at $\eta(a,b) >> 1$ and then the following well-known relationship can be obtained.

$$T \approx \exp(-2\eta(a,b)) = \exp\left(-\frac{4\pi}{h}\int_a^b \sqrt{2m(U(x)-E)}dx\right) \tag{56}$$

Equation (56) is termed as the Gamow permeability factor, which has been used to evaluate the tunnel effect.

$U(x)$ in Eq. (56) may be given as a complicated function such as Eq. (8) in Ref. Sheng (1980) to represent the actual potential barrier. When $U(x)$ in Eq. (56) is given by a rectangular potential with U_o, the values of T at $b-a$ = 1 nm are 3.5467×10^{-5} at U_o = 10 eV and E = 9 eV and 3.9150×10^{-2} at U_o = 10 eV and E = 9.9 eV, respectively. The calculated values are different from the corresponding reasonable values in Exercise calculated by Eq. (16).

Tunnel current at absolute temperature

Before discussing tunnel current, it must be recognized that the tunnel current cannot be calculated directly based on the transmittance T in Eq. (56) and/or Eq. (55) and further consideration is needed. The prerequisite to cause tunneling current needs a potential difference between the two electrodes as shown in Figure 5. This section refers to tunnel current by using a similar diagram as given by Simmons (1963).

Among the electrons in the electrode 1, shown in Figure 5, let's calculate the number of conduction electrons which can arrive at the unit area of electrode surface joined with insulator. Among the conduction electrons, within unit time, the number of the conduction electrons with momentum p_x along the x direction is defined as $n(p_x)$.The possibility of conduction electrons being transferred from the surface of electrode 1 to the surface of the electrode 2. beyond the potential barrier, is given by $T(E_x)$ based on the concept that T in Eq. (56) is represented as a function (see Eq. (SIII-6)) of energy along the x direction.

Thus, the number of electrons N, transferred during unit time, is given by

$$N = \int T(E_x)dn(p_x) \tag{57}$$

The electron number $\Delta n'(p_x)$ with momentum component along the x direction in the range $p_x \sim p_x + \Delta p_x$ is given by the multiplying the density of the quantum state $D(p_x)$ and the Fermi distribution function $f(E)$ representing possibility of the average particle number at each quantum state, which is given by

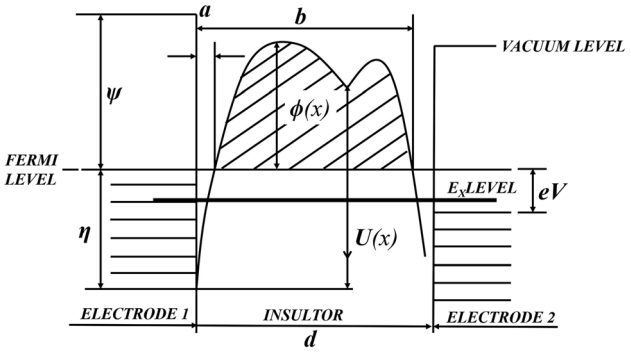

Figure 5: General barrier in insulating film between two metal electrodes (Simmons, 1963).
a, b: limits of barrier at Fermi level, $\Delta d = b - a$; η: Fermi level Ψ: work function of metal electrode; d: the thickness of the insulator film.

$$\Delta n'(p_x) = D(p_x)\Delta p_x f(E) \tag{58}$$

Equation (58) indicates that $D(p_x)\Delta p_x$ means that the number of quantum states with momentum along the x direction in the range $p_x \sim p_x + \Delta p_x$ and $f(E)$ corresponds to Fermi state $F_1(E)$ at electrode 1 associated with the conduction band. The generation of tunnel phenomenon is attributed to a potential difference between the two electrodes. This indicates the existence of Fermi state $F_2(E)$ at electrode 2 which accepts electrons after tunneling, where electrons are Fermi particles with spin quantum number of 1/2.

Representing volume element as $\Delta\Gamma$ for the electron system occupied in phase space, the number of quantum states is given by $2\Delta\Gamma/h^3$ based on the concept that the degree of freedom in real space is 3 and two electrons occupy the same energy level as a pair because of (1/2) spin. The phase space of volume element $\Delta\Gamma$ is given by

$$\Delta\Gamma = \Delta x\Delta y\Delta z\Delta p_x\Delta p_y\Delta p_z \tag{59}$$

The number of quantum states $D(p_x)\Delta p_x$ in the range of $p_x \sim p_x + \Delta p_x$ is given by

$$D(p_x)\Delta p_x = \frac{2}{h^3}\Delta x\Delta y\Delta z\Delta p_x\Delta p_y\Delta p_z \tag{60}$$

Substituting Eq. (60) into Eq. (58), the number of electrons with momentum component in the range of $p_x \sim p_x + \Delta p_x$ can be obtained. However, it should be noted that $\Delta n(p_x)$ in Eq. (57) is the electric number which can reach the surface unit of electrode 1 in contact with the insulator and then the value of Δx is limited by p_x as follows:

$$\Delta x \le u_x\Delta t = \frac{p_x}{m}\Delta t \tag{61}$$

where u_x is the velocity along the x direction. Equation (61) indicates that the electrons existed in the range $\Delta x > u_x\Delta t = p_x\Delta t/m$ can't arrive at the surface of the electrode 1. Thus Eq. (60) is rewritten as follows:

$$D(p_x)\Delta p_x \le \frac{2p_x}{mh^3}\Delta t\Delta y\Delta z\Delta p_x\Delta p_y\Delta p_z \tag{62}$$

Based on Eq. (62), the number of electrons $\Delta n''(p_x)$ is represented as Eq. (63), by considering the potential difference against the opposite side (the electrode 2) to accept electrons tunneled from the electrode 1. That is, $\Delta n''(p_x)$ is the number of electrons which arrive at the surface of $\Delta y\Delta z$ within the time period of Δt.

$$\Delta n''(p_x) = \frac{2p_x}{mh^3}\Delta t\Delta y\Delta z\Delta p_x\Delta p_y\Delta p_z F_1(E)\{1 - F_2(E)\} \tag{63}$$

Thus, the number of electrons $\Delta n(p_x)$ arriving at unit area within unit time period is given as follows:

$$\Delta n(p_x) = \frac{2p_x}{mh^3}\Delta p_x\Delta p_y\Delta p_z F_1(E)\{1 - F_2(E)\} \tag{64}$$

Substituting Eq. (64) into Eq. (57) and integrating for p_x, p_y and p_z, N_1 corresponding to the number of electrons transferred from the electrode 1 to the electrode 2 is given by

$$N_1 = \frac{2}{mh^3}\int_0^{p_{\max}} T(E_x)F_1(E)\{1 - F_2(E)\}p_x dp_x \int_{-\infty}^{\infty} dp_y \int_{-\infty}^{\infty} dp_z \tag{65}$$

By using the velocity u as like Simmons (1963),

$$N_1 = \frac{2m^3}{h^3}\int_0^{u_{\max}} T(E_x)u_x du_x \int_{-\infty}^{\infty} F_1(E)\{1 - F_2(E)\}du_y \int_{-\infty}^{\infty} du_z \tag{66}$$

The integration for Eq. (66) is represented by using $u_r^2 = u_y^2 + u_z^2$ in polar coordinates and by using $E_r = (1/2)mu_r^2$ and $du_y\, du_z = 2\pi u_r\, du_r$, and then it is given as follows:

$$N_1 = \frac{4\pi m^2}{h^3} \int_0^{u_{\max}} T(E_x) u_x du_x \int_0^{\infty} F_1(E)\{1 - F_2(E)\} u_r du_r = \frac{4\pi m^2}{h^3} \int_0^{E_{\max}} T(E_x) dE_x \int_0^{\infty} F_1(E)\{1 - F_2(E)\} dE_r \tag{67}$$

The number N_2 of electrons, tunneled from the electrodes 2 to the electrode 1, is determined by the method similar to N_1.

$$N_2 = \frac{4\pi m^2}{h^3} \int_0^{E_{\max}} T(E_x) dE_x \int_0^{\infty} F_2(E)\{1 - F_1(E)\} dE_r \tag{68}$$

The net flow of electrons N (= $N_1 - N_2$) through the barrier is given by

$$N = \int_0^{E_{\max}} T(E_x) dE_x \left\{ \frac{4\pi m^2}{h^3} \int_0^{\infty} [F_1(E) - F_2(E)] dE_r \right\} \tag{69}$$

When $F_1(E)$ is written as $f(E)$ and the electrode 2 is associated with a positive potential eV with respect to the electrode 1, $F_2(E)$ is written as $f(E + eV)$ by considering the contact potential difference. Then,

$$N = \int_0^{E_{\max}} T(E_x) dE_x \left\{ \frac{4\pi m^2}{h^3} \int_0^{\infty} [f(E) - f(E + eV)] dE_r \right\} \tag{70}$$

As described already, the concept of absolute temperature described by Simmons (1963) has been quoted generally in a number of papers.

Accordingly, tunnel current density J is written by using charge electron e as follows:

$$\begin{aligned} J = eN &= \int_0^{E_{\max}} T(E_x) dE_x \left\{ \frac{4\pi m^2 e}{h^3} \int_0^{\infty} [f(E) - f(E + eV)] dE_r \right\} \\ &= \int_0^{E_{\max}} T(E_x) \zeta dE_x \end{aligned} \tag{71}$$

where $\zeta = \zeta_1 - \zeta_2$. ζ_1 and ζ_2 are given by

$$\zeta_1 = \frac{4\pi m^2 e}{h^3} \int_0^{\infty} f(E) dE_r \tag{72-1}$$

$$\zeta_2 = \frac{4\pi m^2 e}{h^3} \int_0^{\infty} f(E + eV) dE_r \tag{72-2}$$

Equation (71) is the general equation to represent tunnel current density and the final concrete formula is given by Eq. (SIII-7-3). Since the rectangular potential barrier provides different shapes under low, inter-mediate, and high voltage stages, Eq. (SIII-7-3) is classified into three stages. The complicated derivation process of tunnel current by Simmons (1963) is introduced in detail in Supplementary material III.

For low voltage range (Case I), tunnel current density J induced as Eq. (SIII-11) in Supplementary material III is given by

$$J = \left[\frac{(2m\phi_o)^{1/2}}{d} \right] \left(\frac{e}{h} \right)^2 V \exp\left[-\frac{4\pi d}{h} (2m\phi_o)^{1/2} \right] \tag{73}$$

Equation (73) satisfies Ohmic law indicating linear relationship between current density (J) and voltage across film (V).

As described in Supplementary material III, Eq. (SIII-7-3) can be written as Eq. (74) for inter-mediate range and as Eq. (75) for high voltage range, respectively, as follows:

Inter-mediate voltage (Case II)

$$\begin{aligned} J = \left(\frac{e}{2\pi h d^2} \right) \left\{ \left(\phi_o - \frac{eV}{2} \right) \exp\left[-\frac{4\pi d}{h} \left(2m \left(\phi_o - \frac{eV}{2} \right) \right)^{1/2} \right] \right. \\ \left. - \left(\phi_o + \frac{eV}{2} \right) \exp\left[-\frac{4\pi d}{h} \left(2m \left(\phi_o + \frac{eV}{2} \right) \right)^{1/2} \right] \right\} \end{aligned} \tag{74}$$

High voltage (Case III)

$$J = \left(\frac{2.2e\phi_o}{8\pi h\Delta d^2}\right)\left\{\exp\left[-\frac{8\pi\Delta d}{2.96h\phi_o}\left(2m\phi_o^3\right)^{1/2}\right] - \left(1+\frac{2eV}{\phi_o}\right)\exp\left[-\frac{8\pi\Delta d}{2.96h\phi_o}\left(2m\phi_o^3\right)^{1/2}\left(1+\frac{2eV}{\phi_o}\right)^{1/2}\right]\right\} \quad (75)$$

Exercise

Let's confirm the dimension of Eq. (73) for current density under low voltage.

$\left[\frac{(2m\phi_o)^{1/2}}{d}\right]\left(\frac{e}{h}\right)^2 V$ is the dimension of current density. That is,

$$\left[\frac{C^2V}{(J\bullet s)^2 m}(kg\bullet J)^{1/2}\right] = \left[\frac{C}{s\bullet m^2}\bullet\frac{CVm}{J^2 s}(kg\bullet J)^{1/2}\right] = \left[\frac{C}{s\bullet m^2}\frac{CV}{J^2}\left(\sqrt{\frac{kg\bullet m}{s^2}}m\bullet J\right)^{1/2}\right]$$

$$= \left[\frac{C}{s\bullet m^2}\frac{CV}{J^2}(N\bullet m\bullet J)^{1/2}\right] = \left[\frac{C}{s\bullet m^2}\frac{J}{J^2}\left(J^2\right)^{1/2}\right] = \left[\frac{C}{s\bullet m^2}\right] = \left[\frac{A}{m^2}\right]$$

$-\left(\frac{4\pi d_o}{h}\right)(2m\phi_o)^{1/2}$ is dimensionless as follows:

$$\left[\frac{m}{J\bullet s}(kg\bullet J)^{1/2}\right] = \left[\frac{1}{J}\left(\frac{kg\bullet m}{s^2}m\bullet J\right)^{1/2}\right] = \left[\frac{1}{J}(N\bullet m\bullet J)^{1/2}\right] = \left[\frac{1}{J}\left(J^2\right)^{1/2}\right] = [1]$$

Therefore, Eq. (73) becomes the dimension of current density. The same dimension is also obtained for Eqs. (74) and (75).

Incidentally, at low voltage, represented by Eq. (73), the area of insulation film is defined as S and tunnel current and resistivity are defined as I and R, respectively. Because of $I = J \bullet S$ and $R = V/I$, RS becomes

$$RS = \frac{1}{\left[\frac{(2m\phi_o)^{1/2}}{d}\right]\left(\frac{e}{h}\right)^2\exp\left[-\frac{4\pi d}{d}(2m\phi_o)^{1/2}\right]} \quad (76)$$

where e (electron charge) = 1.602×10^{-19} (C), $m = 9.109\times10^{-31}$ (kg), $h = 6.626\times10^{-34}$ (J · s) are intrinsic values. Assuming $d = 10$ Å (10^{-10} m) and $\phi_o = 1$ $eV = 1.602\times10^{-19}$ J for exercise of the numerical calculation, RS becomes 8.917 $\Omega\cdot\mu m^2$. The relationship between barrier width (d) and barrier height (ϕ_o) at the indicated values of RS is shown in Figure 6 (Ohmukai & Hirata, 2006).

Incidentally, the well-known treatment by Simmons (1963) is based on the elastic tunnel current and the inelastic tunnel current such as excitation of the metal phonon is out of the framework. Even so, the slightly simple treatment by Simmons has been well-known and has been adopted for the analyses of scanning tunneling microscope (STM) (Binnig, Rohrer, Gerber, & Weibel, 1992; Stip, Rezaei, & Ho, 1998; Tersoff & Hamann, 1983) and gate current (Dennard, Gaensslen, Rideout, Bassous, & LeBlance, 1974).

However, the conductivity of polymer-conductive filler composites increases with elevating temperatures, when the polymer has high heat resistivity with negligible thermal expansion. To analyze such a phenomenon, the thermal fluctuation-induced tunneling effect by Sheng (1980) must be understood.

Thermal fluctuation-induced tunneling effect

The well-known discussion described above is attributed to the tunnel current at absolute temperature. However, the conductivity of polymer-filler composites, the filler being conductive and the matrix being insulative, is sensitive to the measured temperature.

To resolve this problem, one approach was proposed in terms of fluctuation-induced tunneling conditions. The study is very important to promote polymer science and polymer engineering field to understand temperature dependence of the conductivity of polymer-filler composites. This section introduces the difficult

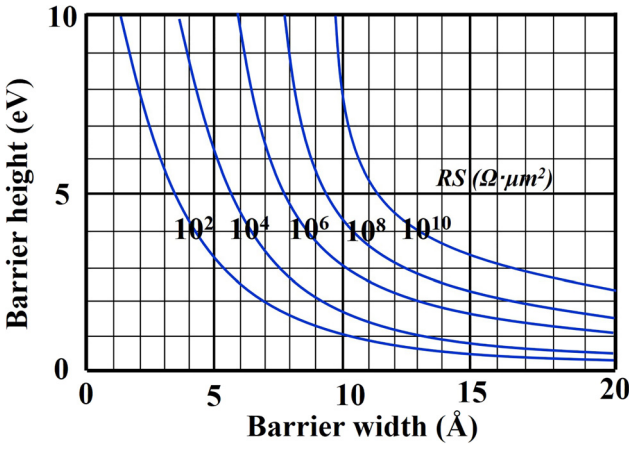

Figure 6: The relationship between barrier width (d) and barrier height (ϕ_o) calculated by Eq. (74) at the indicated RS (Ohmukai & Hirata, 2006).

theory proposed by Sheng (1980) through the detailed derivation of equations up to Eq. (83), described mainly in Supplementary material IV to bridge the gap between education and research. Because polymer scientists have never referred to the quantitative analysis of temperature dependence on conductivity.

Recently, the quantitative analyses have been reported for several kinds of composite (Jonscher, 1977; Zhang, Bin, Dong, & Matsuo, 2014; Zhang, Bin, Zhang, & Matsuo, 2014; Zhang, Bin, Zhang, & Matsuo, 2017). This section focuses on the application limit of an ideal theory to polymer composites with complicated morphology in terms of educational concepts. The application limit is discussed in relation to complex impedance extrapolated to frequency → 0. Before discussing this, we shall refer to thermal fluctuation-induced tunneling effect.

As discussed already, the theory by Simmons (1963) is based on an ideal concept that two electrodes are separated by a thin insulation film and current flows between the unite area of two electrodes, while the theory by Sheng (1980) is based on an ideal tunnel junction of a parallel-plate capacitor with distance d (w in Ref. Sheng, 1980) and area A. Hence the theory by Sheng is suitable for the application to tunnel current for polymer-filler composites. That is, the distance between the parallel-plates of a capacitor corresponds to the distance d between conductive fillers and the plate area corresponds to the surface area A on the filler over which most of tunneling occurs. This concept provides an advantage for evaluating the temperature dependence of d and A, which will be discussed later. The detailed validity is discussed in the next Section "*Application limit of tunnel current theory to polymer-filler composite*" and Supplementary material V.

Sheng approximated such a tunnel junction by a parallel-plate capacitor with area A and separation d shown in Figure 7a, in which C denotes only a small part of the total capacitance C_o between the two large conducting segments given as $A/4\pi d$ and $R/2$ represents the resistivity connecting the junction capacitor to the rest of the conducting segments. A is the area over which most of tunneling occurs.

The point emphasized in this paper is the concept that the barrier between adjacent fillers is associated with the image-forced corrected rectangular barrier as illustrated in Figure 7b. The distance d in Figure 7b corresponds to the distance D for one tunnel junction point as shown in Figure 2c and d. But there exist many gaps with individual D within the composites. Therefore, in the polymer-filler composites, D for the composite means the average effective gap distance that allows effective electron transfer. Therefore, d appeared in the following equations is thought to correspond to the average gap distance D. Incidentally, the energy difference of Fermi levels at electrodes 1 and 2 is given by $\bar{\delta}U_o$ in accordance with the theory by Sheng (1980).

When $C << C_o$, $\langle V_T^2 \rangle$ is given by

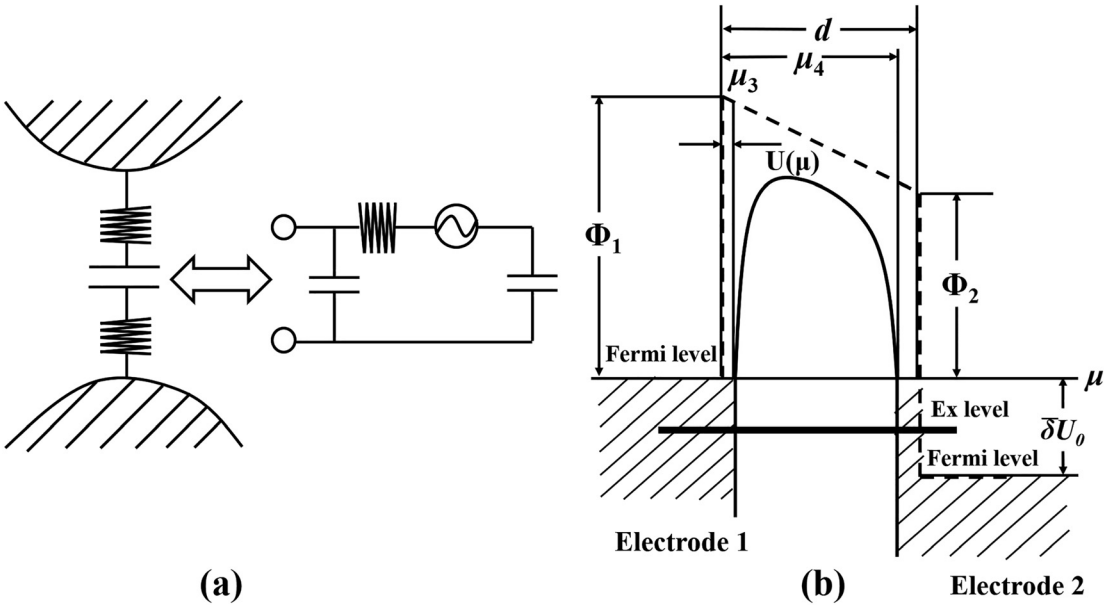

Figure 7: (a) A region of close approach between two conducting (Sheng, 1980). Shaded area denotes conductors. The heavy lines delineate the surface areas where most of the tunneling occurs. (b) General barrier between adjacent conductive fillers, in which the schematic system corresponds to parallel-plate capacitor. Electrons transfer from the left filler (named as electrode 1) to the right filler (named as electrode 2). Φ_1 and Φ_2 are working functions of electrodes 1 and 2, respectively.

$$\begin{aligned}\langle V_T^2\rangle &= \int_0^\infty \frac{4kTR}{(2\pi fCR)^2 + \left(1+\frac{C}{C_o}\right)^2} df \approx \int_0^\infty \frac{4kTR}{(2\pi fCR)^2+1} df \\ &= 4kTR\sqrt{\frac{1}{(2\pi CR)^2}}\left[\arctan\left(\sqrt{(2\pi fCR)^2}\right)\right]_0^\infty = \frac{4kTR}{2\pi CR}\arctan\,[2\pi fCR]_0^\infty \\ &= \frac{2kT}{\pi C}\left[\arctan(\infty) - \arctan(0)\right] = \frac{2kT}{\pi C}\times\frac{\pi}{2} = \frac{kT}{C}\end{aligned} \tag{77}$$

Following Sheng (1980), the equipartition theory is a direct consequence of the Boltzmann distribution and then the above equation suggests that the probability of fluctuations is proportional to $\exp(-\Delta E/kT)$ associated with the energy needed to move the system away from equilibrium. From this concept, the normalized function of fluctuation probability for $0 \le \delta_T < \infty$ is given by

$$P(\delta_T) = \sqrt{\frac{4a}{\pi kT}}\exp\left(-\frac{a\delta_T^2}{kT}\right) 0 < \delta_T < \infty \tag{78}$$

Temperature dependence of tunnel current is attributed to the thermal fluctuation voltage field V_T and field $\delta_T (= V_T/d)$ across the tunnel junction d in addition to externally applied voltage V_A and applied field $\delta_A (= V_A/d)$. The actual theoretical analysis for partial conductivity by using net tunnel current Δj along the direction of applied field is defined as

$$\begin{aligned}\sum(\delta_T) &= \lim_{\delta_A\to 0}\frac{\Delta j}{\delta_A} \\ &= \lim_{\delta_A\to 0}\frac{\frac{d}{d\delta_A}\left(\frac{1}{2}\left[j(\delta_T+\delta_A) - j(\delta_T-\delta_A)\right]\right)_{\delta_A=0}}{(\delta_A)'} = \frac{\left(\frac{1}{2}\left[j'(\delta_T+\delta_A) - j'(\delta_T-\delta_A)\right]\right)_{\delta_A=0}}{1} \\ &= j'(\delta_T) = \frac{dj(\delta_T)}{d\delta_T}\end{aligned} \tag{79}$$

The fluctuation-induced tunneling conductivity $\sigma(T)$ of the junction is then obtained by using thermal averaging $\sum(\delta_T)$ as follows:

$$\sigma(T) = \int_0^\infty P(\delta_T)\sum(\delta_T)d\delta_T = \int_0^\infty P(\delta_T)\frac{dj(\delta_T)}{d\delta_T}d\delta_T \tag{80}$$

As discussed already, the barrier between adjacent fillers is associated with the image-forced corrected rectangular barrier at one joint point as illustrated in Figure 7b and there exist many gaps with similar potential barrier in the composites.

The accurate potential barrier function is expressed as Eq. (81) by Sheng, in which the notations $V(u,\overline{\delta})$ and V_o in Ref. Sheng (1980) are represented as $U(u,\overline{\delta})$ and U_o, respectively, in this paper.

$$U((u,\overline{\delta}) = U_o\left[1 - \frac{\lambda}{u(1-u)} - \overline{\delta}u\right] = U_o\left[1 - \frac{\lambda}{u(1-u)} - \epsilon\overline{\delta}_o u\right] \tag{81}$$

where $u = x/d$ is the reduced spatial variation and x is the distance from the left surface of the junction. U_o is the height of the rectangular potential barrier in the absence of image-force correction and $\overline{\delta} = \delta ed/U_o$ is the electric field expressed in units of $\delta_U = U_o/ed$. The peaked curve profile of Eq. (81) can be drawn roughly in Figure 7b as the pattern diagram, in which the adjacent fillers are termed as electrodes 1 and 2 to facilitate easy understanding in relation to the previous sections. The maximum peak is denoted by $U_{\max} = U(u*,\overline{\delta})$ and $u^\star$ satisfies the condition $(\partial U/\partial u) = 0$. The condition reveals the decreasing function of $\overline{\delta}_o$ against λ (Sheng, 1980).

Furthermore,

$$\lambda = \frac{0.795e^2}{4dKU_o} \tag{82}$$

λ is the dimensionless parameter governing the amount of image-force correction and the barrier shape, in which e is the electric charge and K is the dielectric constant of the insulating barrier. Based on $U_{\max}$ calculated from a given λ, $\overline{\delta} = \overline{\delta}_o$ is defined. $\overline{\delta}_o = 0$ at $\lambda = 1/4$, in which $U_{\max} = 0$. This indicates that $\lambda > 1/4$ is out of framework of the concept about tunnel current. As discussed by Sheng, a new dimensionless field parameter is defined as $\epsilon = \overline{\delta}/\overline{\delta}_o$. The parameter is very convenient to characterize the electric field. That is, $\epsilon = 1$ marks the point below which $U_m \geq 0$ and above which $U_m \leq 0$. The theoretical calculation indicated that tunneling characteristics for $\epsilon \leq 1$ are drastically different from those for $\epsilon > 1$ (Zhang, Bin, Zhang, et al., 2014; Zhang et al., 2017).

Eqs. (79) and (80) can be represented by using $\epsilon = \overline{\delta}/\overline{\delta}_o$ as follows:

$$\sum(\epsilon) = \frac{1}{\delta_o}\frac{dj(\epsilon)}{d\epsilon} \tag{79}'$$

$$\sigma = \int_0^\infty P(\epsilon)\frac{dj(\epsilon)}{d\epsilon}d\epsilon = \delta_o\int_0^\infty P(\epsilon)\sum(\epsilon)d\epsilon = \sigma(T) \tag{80}'$$

Also, Eqs. (78) and (81) are given as follows:

$$P(\epsilon) = \left(\frac{4a}{\pi kT}\right)^{1/2}\exp\left[-\frac{a\epsilon^2}{kT}\left(\frac{\overline{\delta}_o U_o}{ed}\right)^2\right] \tag{78}'$$

and

$$U(u,\epsilon) = U_o\left[1 - \frac{\lambda}{u(1-u)} - \overline{\delta}_o\epsilon u\right] \tag{81}'$$

$P(\epsilon)$ is a function of temperature T and then σ is represented as $\sigma(T)$.

The final equation about temperature dependence of conductivity $\sigma(T)$ is given by

$$\sigma((T) = \delta_o \int_0^\infty P(\epsilon_T)\sum(\epsilon_T)d\epsilon_T$$
$$= \left(\frac{4T_1}{\pi T}\right)^{\frac{1}{2}}\left[\int_0^1 \sum_o(\epsilon_T)\exp\left(-\frac{T_1}{T}\epsilon_T^2 - \frac{T_1}{T_o}\varphi(\epsilon_T)\right)d\epsilon_T + \int_1^\infty \sum_1(\epsilon_T)\exp\left(-\frac{T_1}{T}\epsilon_T^2\right)d\epsilon_T\right] \quad (83)$$

$$T_1 = \frac{a\delta_o^2}{k} = \frac{\left(\overline{\delta}_o U_o\right)^2}{8\pi k e^2}\left(\frac{A}{d}\right) \quad (84\text{-}1)$$

$$T_o = \frac{T_1}{2\chi d\xi(0)} = \frac{h\left(\overline{\delta}_o U_o\right)^2}{32\pi^2 k e^2 (2mU_o)^{1/2}\xi(0)}\left(\frac{A}{d}\right) \quad (84\text{-}2)$$

$$\varphi(\epsilon) = \frac{\xi(\epsilon)}{\xi(0)} \quad (84\text{-}3)$$

where $\varphi(0) = 1$ and $\varphi(1) = 0$.

This section refers to only the outline to derive Eq. (83) and the detailed derivation process is represented in Supplementary material IV. The derivation for many equations in Sheng's paper is very difficult for most of polymer scientists, as the detailed derivation of each equation is needed.

Furthermore, Supplementary material IV provides the method to determine the optimum values of important parameters of d and A by computer. The parameter fitting process for ensuring good agreement of the parameters in Eq. (83) with experimental results is slightly complicated (Zhang, Bin, Dong, et al., 2014; Zhang, Bin, Zhang, et al., 2014; Zhang et al., 2017). As an example, the pursued fitting method is described by using well-dispersed vapor grown carbon fiber (VGCF) within polyimide (PI) matrix (Zhang et al., 2017), since VGCFs like rigid CFs, provide higher conductivity than carbon black at the lower filler content (see Figure S5 in Supplementary material V). This composite is suitable for Sheng's theory associated with low applied field. PI used as the matrix, is a rigid amorphous polymer with negligibly small thermal expansion up to 180 °C.

Now, we shall refer to the reason as to why PI is selected as the matrix, although PI is independent of PTC effect. Certainly, PTC effect is related to tunnel current but PI is better as matrix to investigate the mechanism about temperature dependence of tunnel current density for polymer-filler composites, since the distance between adjacent fillers is thought to be constant independent of the measured temperature. Accordingly, the PI-VGCF composites were adopted to pursue the easy explanation about temperature dependence of tunnel current in terms of educational concept.

Figure 8 shows the results for the PI/VGCF composites with 3.11 vol% VGCF content corresponding to the critical concentration and with 6.28 vol% VGCF content (Zhang et al., 2017). The composites were pressed to assure constant thickness under high pressure before measuring the temperature dependence of current versus the indicated voltages. The good fitting for conductivity at the indicated temperatures could be achieved at the optimum values of the parameters in columns (c) and (d), respectively.

The calculated values of average distance D in columns (c) and (d) in Figure 8 are 1.20 and 1.00 nm for the composites with 3.11 and 6.28 vol% contents, respectively, which means the average distance D shown in column (d) in Figure 2. The average distance D to allow electron transfer is essentially different from d in Figure 7b given by the ideal system but D is thought to be equal to d to pursue the theoretical calculation.

On the parameter fitting process, it was found that d is very sensitive to the conductivity in comparison with the other parameters. Without setting optimum value of d, the calculated values deviate greatly from the experimental result. The value of λ calculated by Eq. (82) is not sensitive to temperature since d is a constant independent of the temperatures. The small change of λ is thought to be due to the slight thermal fluctuation of U_o attributed to applied voltage and VGCF contents. Accompanying the slight change in λ, $\overline{\delta}_o$ slightly depends on temperature. The parameter fitting indicated that an increase in area A is attributed to an increase in conductivity of the composite, which is shown in columns (e) and (f) in Figure 8.

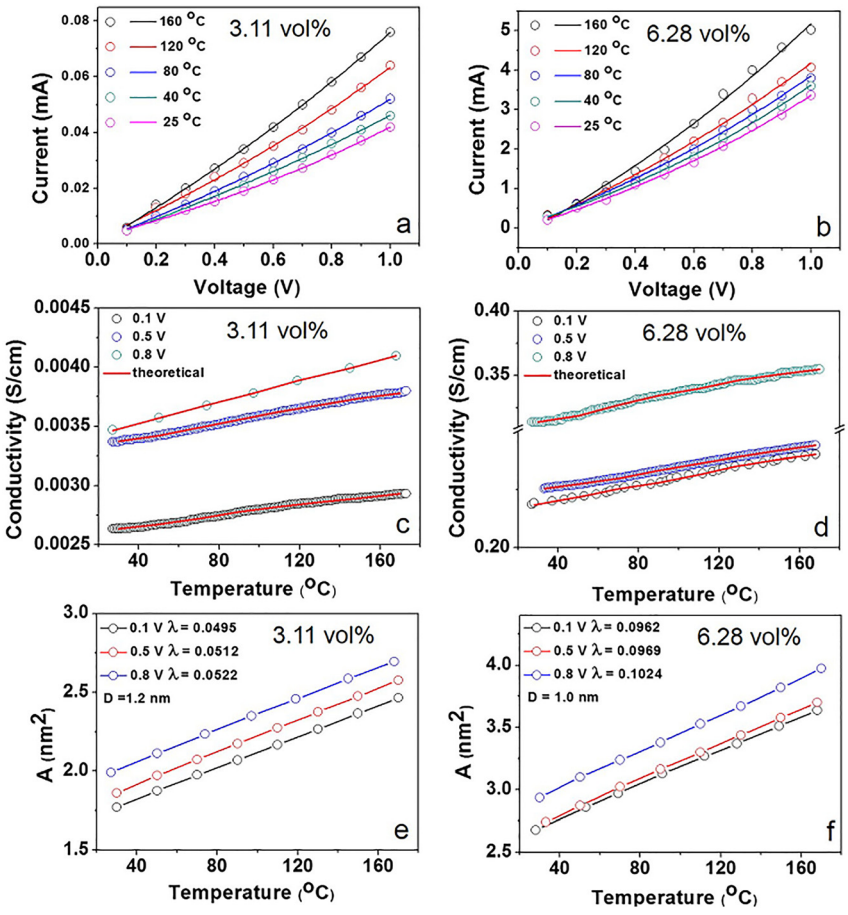

Figure 8: (a) and (b): Current versus voltage for PI/VGCF composite with 3.11 vol% and 6.28 vol% contents at the indicated temperatures, respectively; (c) and (d): Experimental and theoretical conductivities versus temperature for PI/VGCF composites with 3.11 and 6.28 vol% contents at the indicated voltages, respectively; (e) and (f): Theoretical value of *A* versus temperature for the composites with 3.11 and 6.28 vol% contents, respectively, which were obtained as the parameter ensuring the good agreement between experimental and calculated results in (c) and (d) (Zhang et al., 2017).

Based on the above postulation for parameter fitting, this paper refers to the concrete parameter fitting process by computer, based on Eqs. (SIV-33) and (SIV-34) in Supplementary material IV.

As the first step, the focus is to determine ϵ_T^* in Eq. (SIV-33). As common sense for tunnel current, the parameter d shown in Figure 7b is set in the range of 0.8–1.5 ($\times 10^{-9}$ m) at the interval of 0.05 ($\times 10^{-9}$ m). The initial stage, λ for each setting value of d is determined by Eq. (82) assuming $U_o = 1$ as the tentative initial value and consequently $\overline{\delta}_o$ can be determined from the relationship between $\overline{\delta}_o$ and λ at $U_{\max}(u, \epsilon) = 0$ (see Figure 4 in Ref. Sheng, 1980). Incidentally, electric charge e, electric mass m, Prank constant h and Boltzmann constant k are 1.602×10^{-19} (C), 9.109×10^{-31} (kg), 6.626×10^{-34} (J· s), and 1.381×10^{-23} (J/K), respectively. The dielectric constant of PI as matrix of the composite with relative permittivity 3.5 at room temperature was calculated with vacuum permittivity 8.854×10^{-12} (F/m) to use Eq. (82).

Based on the values of λ and $\overline{\delta}_o$ calculated for each value of d (0.8–1.5 nm), $\xi(\epsilon)$ can be obtained by integration of Eq. (SIV-10) at a fixed value of ϵ_T^* for u in the range from u_3 to u_4 at integrated interval 0.01. As the same procedure in Figure S4 in Supplementary material IV, the value of ϵ_T^* to give the maximum value of $-\varphi(\epsilon_T) - \epsilon_T^2$ is determined from λ. Concretely, the value of λ is determined by the individual value of d (0.8–1.5 nm) using Eq. (82), when U_o is selected to be unity as the initial tentative value.

As the second step, $\varphi(\epsilon_T^*)(= \xi(\epsilon_T^*)/\xi(0))$ can be obtained by using ϵ_T^*. Thus, Eq. (SIV-33) is represented as a function of T. The theoretical curves by Eq. (SIV-33) must be compared with the experimental results measured at 25, 40, 80, 120 and 160 °C (Zhang et al., 2017).

Through the curve fitting, the optimum values of T_o, T_1 and σ_o are obtained for the composites with 3.11 and 6.28 vol% contents. Since d is set in the range 0.8–1.5 ($\times 10^{-9}$ m) at the interval of 0.05 ($\times 10^{-9}$ m) as discussed above, the individual A value can be determined tentatively for individual d values by using Eq. (82)

and Eqs. (SIV-30)–(SIV-32). Also corresponding $\overline{\delta}_o$ is determined by λ (see Figure 4 in Ref. Sheng, 1980). In this parameter fitting stage, using Eq. (SIV-33), the d value is confirmed to be very sensitive to the conductivity but it must be almost same, independent of the measured temperature because of no dimensional change in bulk. To satisfy independence of temperature about d, the values of d are determined to be ca. 1.20 and 1.00 nm for the composites with the 3.11 and 6.28 vol% contents, respectively by modifying the meters scale. On selecting values different from the above d values, it was found that the calculated conductivity deviates from the experimental one. On the other hand, the value of A, determined by Eq. (SIV-30) or Eq. (SIV-31), is confirmed to be larger with increasing temperature, because of slight temperature dependence of U_o and λ.

As the final step, the values of A, U_o and λ obtained by Eq. (SIV-33) as the initial tentative values are substituted into Eq. (SIV-29) to pursue further better fitting between the calculated and experimental results at the fixed values d (fixed at 1.20 and 1.00 nm).

The integration by ϵ_T was with an interval of 0.01, in which the complicated calculation parts concerning Eq. (SIV-26-1), by using commercial program for the differentiations on the figures about $d\xi(\epsilon)/d\epsilon$ and $d[\eta_o(\epsilon)]/d\epsilon$, were incorporated in the original program. The detailed numerical calculation is done by trial and error, using a computer, till the best fitting can be obtained. The results are shown in Figure 8e and f.

Incidentally, the fitting was done for the first term in Eq. (SIV-29). The second term for $\epsilon_T > 1$ was much smaller than the first term at $\epsilon_T = 1$ and the non-integral function decreased drastically with increasing ϵ_T beyond unity.

As analyzed by Sheng (1980), the difference at $\epsilon_T = 1$ is attributed to the artifact of $T(E, \epsilon)$ given by Eq. (SIV-8), which is attributed to the variation of approximation of $T(E, \epsilon)$ at $E = U_m$ by an abrupt slope change.

Let's refer to the big problem about the evaluation of tunnel current by DC measurement. As described in this paper, the application of the tunnel current theory (Sheng, 1980) to the complicated system, the conductive fillers being dispersed uniformly in insulator matrix, is allowed only to such a limited system that the resistivity between the adjacent fillers is much higher than the resistivity interface between bulk and electrode and the resistivity by carrier movement within the fillers. In this case, the average distance D between adjacent fillers in Figure 2d may be almost equal to d, although the distance D is generally different from a very thin insulation film thickness d between parallel-plate capacitors. Certainly, it may be postulated that the area A shown in Figure 2d probably corresponds to a parallel-plate as a capacitor described by Sheng. This is the most important subject, although most of papers by polymer scientists have never referred to the limit on analyzing electric properties of polymer-filler composite in terms of tunnel current. Section "*Application limit of tunnel current theory to polymer-filler composite*" in the paper and Supplementary material V refer to the reason in terms of impedance at frequency → 0 by DC component of AC measurement in detail.

Application limit of tunnel current theory to polymer-filler composite

Again, it should be emphasized that if the resistivity of the PI-VVGCF composite is not strongly affected by the average resistivity between adjacent VGCFs, the measured density current of the composite is independent of tunnel current density. Namely, the value of d calculated by Eq. (83) using the measured current density becomes meaningless, which is independent of the accurate value of D shown in Figure 2d. Even so, it may be justified that D is almost equivalent to the calculated d only in the case where (i) the resistivity between adjacent VGCFs is much higher than the other two, that is, (ii) interference resistivity between electrode and composite and (iii) the resistivity of VGCFs themselves shown in Figure 10c later. Incidentally, the consideration about the two factors (ii) and (iii) is unnecessary for the reported ideal model systems (Sheng, 1980; Simmons, 1963).

It is well-known that the conductivity of the composite by DC measurements is generally attributed to three kinds of resistivity, (i), (ii), and (iii).

To demonstrate extremely high resistivity between adjacent fillers in comparison with the other two resistivity factors, this paper provides one approach to evaluate the DC component by AC measurement at frequency → 0 Hz. To pursue this approach, the frequency dependence of complex impedance (Z^*) were measured for the composites with 3.11 and 6.28 vol% contents under 0.1 and 0.5 V.

Figure 9 shows one of the examples for the composite with 6.28 vol% content, in which frequency dependence of Z′ and Z″, Cole-Cole plots, and AC conductivity κ (real part) were evaluated at the indicated temperatures under 0.1 V. The experimental and theoretical results are shown as plots and curves, respectively (Zhang et al., 2017).

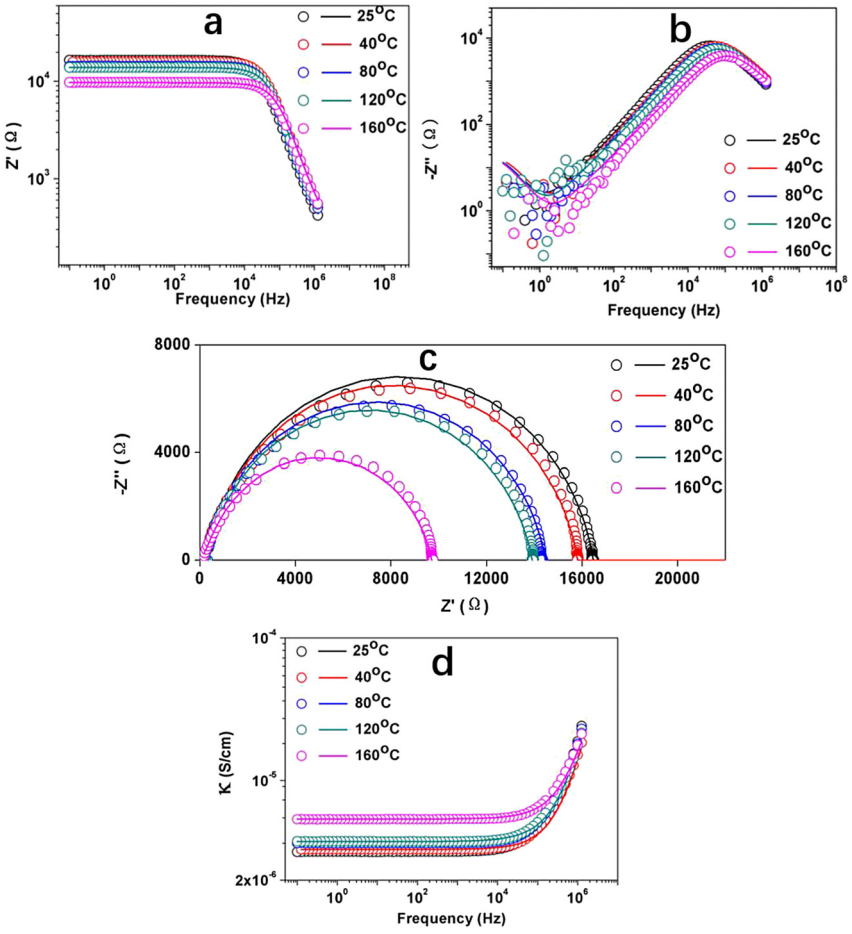

Figure 9: (a) and (b); Frequency dependence of Z' and Z''; (c) Cole-Cole plots for Z^*; (d) Frequency dependence of AC conductivity (κ). Open circles: experimental results. Solid lines: theoretical results. All results at the indicated temperatures were obtained for the composite with 6.28 vol% content under 0.1 V. Incidentally, the imaginary part κ'' is negligibly small in comparison with real part κ (Zhang et al., 2017).

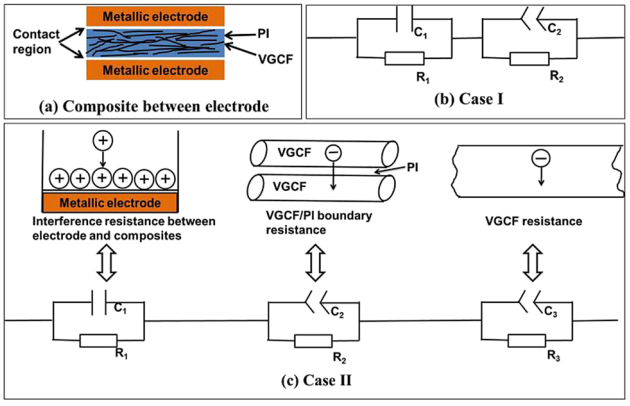

Figure 10: (a) Composite between electrodes; (b) an equivalent circuit with two units for the PI/VGCF composite with 3.11 vol% content; (c) an equivalent circuit with three units for the PI/VGCF composite with 6.28 vol% content. The first unit: interface between bulk and electrode: the second unit: interface between adjacent VGCFs inserting PI; the third unit: carrier movement within VGCFs.

For Z* in Figure 9a and b, the experimental plots at the indicated temperatures are almost overlapped. The frequency dependence curves of Z' can be distinguished into two regions, plateau region below ca. 10^4 Hz and drastically decreasing region beyond ca. 10^4 Hz. The frequency of peak appearance for Z'' in Figure 9b is related to the frequency corresponding to the drastic decrease of Z'. The peak of Z'' shifts to higher frequency with increasing temperature but the difference is not considerable. The Z″ increases with decreasing frequency in the lower frequency range. The duller decrease of Z'' may be consisted of several relaxations. Each Cole-Cole plot of Z^* at the indicated temperatures in Figure 9c shows a circular arc, which is independent of the measured temperatures, but slightly deviates from the arc at low frequency side (higher value side of Z'). Judging from smooth plots of the experimental results of Z′ and Z″, the κ values in Figure 9d calculated from Z*, are thought to ensure the high creditability.

To demonstrate extremely high resistivity between adjacent fillers (VGCF/PI boundary region) in comparison with other resistivities, the schematic model for calculating impedance of the system is proposed in Figure 10. AC measurement has the advantage that resistivity of the composite can be classified into the several contributions by equivalent circuits. The resistivity of the composite with 3.11 vol% content is classified into two, the interference resistivity (R_1) between electrode and composition, and the filler-matrix boundary resistivity (R_2) indicating resistivity between adjacent fillers inserting PI (see Case I). The resistivity for the composite with 6.28 vol% content is classified into three components, the filler resistivity (R_3) associated with carrier movement within the filler in addition to R_1 and R_2 (see Case II). If filler-matrix boundary resistivity R_2 indicating resistance between adjacent fillers inserting PI is much higher than other two R_1 and R_3, the measured resistivity at frequency → 0 Hz corresponds to the DC resistance attributed to filler-matrix boundary resistance. To evaluate the three kinds of resistivity, the impedance as a function of frequency was evaluated by using the equivalent circuit models. The contribution to resistance of DC component in Case I and Case II can be evaluated by extrapolating frequency → 0 Hz.

Incidentally, the adoption of the different units for the two composites is discussed in Supplementary material V. The impedance of the equivalent circuit with two or three units is given by

For Case I

$$\begin{aligned} Z^* &= \frac{1}{\frac{1}{R_1} + i\omega C_1} + \frac{1}{\frac{1}{R_2} + (i\omega)^{\alpha} C_2} = Z_1^* + Z_2^* \\ &= Z_1' - iZ_1'' + Z_2' - iZ_2'' = (Z_1' + Z_2') - i(iZ_1'' + iZ_2'') = Z' - iZ'' \end{aligned} \tag{85-1}$$

For Case II

$$\begin{aligned} Z* &= \frac{1}{\frac{1}{R_1} + i\omega C_1} + \frac{1}{\frac{1}{R_2} + (i\omega)^{\alpha} C_2} + \frac{1}{\frac{1}{R_3} + (i\omega)^{\beta} C_3} = Z_1^* + Z_2^* + Z_3^* \\ &= Z_1' - iZ_1'' + Z_2' - iZ_2'' + Z_3' - iZ_3'' = (Z_1' + Z_2' + Z_3') - i(Z_1'' + Z_2'' + Z_3'') = Z' - iZ'' \end{aligned} \tag{85-2}$$

Among C_1, C_2 and C_3, C_2 and C_3 are the true capacitances of the contact region associated with CPE. The CPE exponents α and β are given as $\alpha = \phi_{CPE}/90°$ and $\beta = \phi_{CPE}/90°$, respectively (Fan et al., 2014; Jonscher, 1977; Zhang et al., 2017; Zhu et al., 2012). Since the phase angle ϕ_{CPE} ($<90°$) is frequency-independent, α and β are also independent of frequency and less than 1.0. When α and β are equal to 1.0, the CPE becomes an ideal capacitor, which is applied to flat surface interference between electrode and composite. The physical contributions of these parameters in Eq. (85) can be proven later via curve fittings with the experimental results.

The procedure for determining components of impedance (Z_1'~Z_3' and Z_1''~Z_3'') is shown in Figure S6 in Supplementary material V. As an example of Z^*, the results for the composite with 6.28 vol% content at 0.1 V are shown as theoretical curves in Figure 9a and b, which are in good agreement with experimental results by selecting optimum values of parameters for R_1, R_2, R_3, C_1, C_2, C_3, α and β. Also, the Cole-Cole plots and the AC conductivity κ are shown as curves in Figure 9c and d, respectively. The optimum values calculated are listed in

Table 1 at the indicated temperature. The other conditions for 6.26 vol% content at 0.5 V and for 3.11 vol% content at 0.1 and 0.5 V are shown as Table S1 and Tables S2–S3, respectively in Supplementary material V.

In Table 1, the values of R_2 (resistivity between adjacent VGCF fillers) are much higher than R_1 (interference resistivity between electrode and composite) and R_3 (VGCF resistivity) in Case II for 6.28 vol% content at $V = 0.1$. Of course, the values of R_2 are reported to be much higher than R_1 in Case I for 3.11 vol% content (Zhang et al., 2017). Accordingly, the values of κ_{DC} are strongly affected by R_2, since κ_{DC} corresponding to the DC component (frequency → 0 Hz) of AC conductivity is represented as $\epsilon_o/\{C_o(R_1 + R_2 + R_3)\}$ for the composite with 6.28 vol% content and as $\epsilon_o/\{C_o(R_1 + R_2)\}$ for the composite with 3.11 vol% content, respectively. The coefficients ϵ_o and C_o are permittivity and capacitance, respectively at frequency → 0 Hz. Namely, the values of κ_{DC} are determined obviously by the value of R_2.

Using the values of κ_{DC}, the values of λ, D, and A are obtained and the results are listed in Table 2. The fitting procedure to obtain the above parameters is also the same as described for DC measurement.

As listed in Table 2, the D values calculated by using κ_{DC} are 1.20 and 1.00 nm for the composites with 3.11 and 6.28 vol% contents, respectively. The values are the same as the values obtained by DC measurement shown in columns (c) and (f) in Figure 8. The λ values calculated are almost independent of the measured temperatures but they depend on the VGCF contents. Namely, the λ values for 3.11 vol% content were 0.0220 independent of temperature, while the values (0.02468–0.02598) for 6.28 vol% content indicate a slight

Table 1: The corresponding parameters R_i (i = 1–3) and C_i (i = 1–3) in Eq. (85-2) obtained by computer simulation for the composites with 6.28 vol% content under 0.1 V at the indicated temperatures.

T (°C)	25	40	80	120	160
R_1 (Ω)	30	30	30	30	30
C_1 (F × 10^{-3})	89.5	89.9	90.0	95.0	100
R_2 (Ω × 10^4)	1.62	1.55	1.42	1.36	0.94
C_2 (pF)	783	800	793	890	920
α	0.893	0.888	0.883	0.874	0.865
R_3 (Ω)	310	308	306	304	300
C_3 (pF × 10^4)	3.40	3.51	3.80	4.08	4.18
β	0.655	0.650	0.625	0.630	0.650

Table 2: Temperature dependence of parameters D, A and λ at 0.1 and 0.5 V calculated by using κ_{DC}.

	T (°C)	λ 0.1 V	D (nm) 0.1 V	A (nm^2) 0.1 V	λ 0.5 V	D (nm) 0.5 V	A (nm^2) 0.5 V
3.11 vol%	25	0.02200	1.20	1.621	0.02216	1.20	1.740
	40	0.02200	1.20	1.701	0.02216	1.20	1.752
	80	0.02200	1.20	1.931	0.02216	1.20	1.912
	120	0.02200	1.20	1.941	0.02216	1.20	2.000
	160	0.02200	1.20	1.977	0.02216	1.20	2.135
	T (°C)	λ 0.1 V	D (nm) 0.1 V	A (nm^2) 0.1 V	λ 0.5 V	D (nm) 0.5 V	A (nm^2) 0.5 V
6.28 vol%	25	0.02468	1.00	2.010	0.02515	1.00	2.360
	40	0.02489	1.00	2.330	0.02531	1.00	2.510
	80	0.02498	1.00	2.430	0.02546	1.00	2.780
	120	0.02501	1.00	2.500	0.02568	1.00	2.860
	160	0.02598	1.00	2.750	0.02582	1.00	2.980

increase with increasing temperature but the variation is very narrow. The difference of λ between the two VGCF contents is thought to be due to the slight decrease of $\overline{\delta}_o$ and U_o, since the conductivity for the 6.28 vol% content is higher than that for the 3.11 vol% content.

At the indicated temperatures, the values of A calculated by using κ_{DC} for the 6.28 vol% content are higher in comparison with those for the 3.11 vol% content. For the two composites, the A value increased with elevating temperature, while D value is constant because of negligibly small size change in the bulk. Thus, an increase in the transfer electron number with increasing temperature is obviously attributed to the expansion of the average surface area over which most of tunneling occurs (Stip et al., 1998; Zhang et al., 2017). Namely, A is related to the number of electrons transferred by tunneling effect associated with conductivity between adjacent VGCFs inserting PI. Incidentally, the above phenomenon indicates that the increase in A is independent of D assuring the flat surface, since the area A is thought to be just very small flat spot on the surface of VGCF.

As an important point, it should be noted that the concept of tunnel current for polymer-filler composite was established by assuming a parallel-plate capacitor proposed by Sheng (1980). As a prerequisite, the application to conductive polymer-filler composite must be limited to the case where the resistivity between adjacent fillers must be much higher than the other two, interference resistivity between electrode and composite and VGCF resistivity. If the polymer chains of the matrix have functional groups, the resistivity between adjacent fillers is not higher than the other two. This indicates that average conductivity of the composite by DC measurement does not reflect the resistivity between adjacent fillers inserting polymer matrix predominantly.

On discussing tunnel current for PI/VGCF composites as a function of the measured temperatures, the constant average distance D between adjacent fillers can justify the application of the composites to the theory by Sheng (1980), since the bulk dimensional change with increasing temperature is zero within the experimental error.

Conclusion

When teaching the electric property of insulation polymer-conductive filler composites at the measured temperatures, the mechanism of electron transfer between adjacent fillers embedded in polymer matrix is important to understand tunnel current. To facilitate understanding the electron transfer, electron transmittance based on rectangular potential barrier was presented by using the one-dimensional Schrödinger wave function. The adoption of the rectangular potential barrier is associated with the smooth connection of the wave functions at each boundary in Section "*Simple application of Schrödinger equation to tunnel effect*". However, actual potential barrier is different and the transmittance for the arbitrary function was represented using the WKB approximation, which is very important to pursue the theoretical calculation of tunnel current. The concept and the detailed deviation were described in Section "*Analysis for tunnel effect using the WKB approximation*" and Supplementary material II, respectively.

By using WKB approximation, the well-known theoretical calculation of tunnel current at absolute temperature by Simmons (1963) was introduced and this paper pointed out that the popular equation represented in textbooks is limited for the low voltage range. And the detailed derivation of the general equation was proposed through complicated mathematical treatment in Supplementary material III.

However, the electric property for polymer-filler composites must be discussed as a function of the measured temperature. Unfortunately, the detailed theoretical calculation for the composites has never been reported. This paper referred to the commentary for the derivation of the difficult equations by Sheng (1980) and proposed the parameter fitting by computer about the average distance D between adjacent fillers and the area A where most of tunneling occur. When applying Sheng's theory to the polymer-filler systems, D may be almost equivalent to the distance d between two-parallel capacitors. Furthermore, the application of the general theory to polymer-filler composites can be realized only in the limited case where the resistivity

between adjacent conductive fillers inserting polymer matrix is much higher in comparison with two kinds of resistivity, (i) interference resistivity between electrode and composite and (ii) resistivity of fillers. The concept was satisfied by the impedance obtained by AC measurement for the PI-VGCF composites with 3.11 vol% and 6.28 vol% VGCF contents. The former and latter distances were 1.2 and 1.0 nm, respectively, which indicated reasonable values. Thus, the above evaluation plays an important role in teaching the electric property of polymer-filler composites.

Author contributions: All the authors have accepted responsibility for the entire content of this submitted manuscript and approved submission.
Research funding: None declared.
Conflict of interest statement: The authors declare no conflicts of interest regarding this article.

References

Bin, Y., Chen, Q., Tashiro, K., & Matsuo, M. (2008). Electrical, thermal, and mechanical properties of iodine-doped highly elongated ultrahigh molecular weight polyethylene films filled with multiwalled carbon nanotubes. *Physical Review B*, *77*(3), 035419.

Binnig, G., Rohrer, H., Gerber, Ch., & Weibel, E. (1992). Surface studies by scanning tunneling microscopy. *Physical Review Letters*, *49*, 57–59.

Dennard, R. H., Gaensslen, F. H., Rideout, V. L., Bassous, E., & LeBlance, A. R. (1974). Design of ion-implanted MOSFET's with very small physical dimensions. *IEEE Journal of Solid-State Circuits*, *9*, 256–268.

Fan, S., Bin, Y., Zhang, R., Zhang, P., Zhu, D., & Matsuo, M. (2014). Dielectric change of copper phthalocyanine and polyurethane foam with high elasticity as a function of pressure discussed in terms of conversion from natural mechanical energy to electric energy. *Macromolecules*, *47*(3), 8281–8294.

Fowler, R. H., & Nordheim, L. M. (1928). Electron emission in intense electric fields. *Proceedings of the Royal Society of London. Series A*, *119*, 173–181.

Gossling, B. S. (1926). The emission of electrons under the influence of intense electric field. *Philosophical Magazine*, *1*(3), 609–635.

Isaji, S., Bin, Y., & Matsuo, M. (2009). Electric conductivity and self-temperature-control heating properties of carbon nanotubes filled polyethylene films. *Polymer*, *50*, 1046–1053.

Jonscher, A. K. (1977). The 'universal' dielectric response. *Nature*, *267*, 673–679.

Koganemaru, A., Bin, Y., Agari, Y., & Matsuo, M. (2004). Composites of polyacrylonitrile-multiwalled carbon nanotubes prepared by gelation/crystallization from solution. *Advanced Functional Materials*, *14*, 842–850.

Millikan, R. A., & Eyring, C. F. (1926). Laws governing the pulling electrons out of metals by intense electrical field. *Physical Review*, *27*(1), 51–67.

Nordheim, L. W. (1928). The effect of the image force on the emission and reflection of electrons by metals. *Proceedings of the Royal Society of London. Series A*, *121*, 626–639.

Ohmukai, M., & Hirata, Y. (2006). Resonant tunneling in a single barrier structure. *Memoirs of Akashi National College of Technology*, *49*, 22–25.

Schottky, W. (1923). Überkalte und warme elektronenentladungen. *Zeitschrift fur Physik*, *14*, 63–106.

Sheng, P. (1980). Fluctuation-induced tunneling conduction in disordered materials. *Physical Review B*, *21*, 2180–2195.

Simmons, J. G. (1963). Generalized formula for the electric tunnel effect between similar electrodes separated by a thin insulating film. *Journal of Applied Physics*, *34*, 1793–1803.

Stip, B. C., Rezaei, M. A., & Ho, W. (1998). Single-molecular vibrational spectroscopy and microscopy. *Science*, *280*, 1732–1735.

Tersoff, J., & Hamann, D. R. (1983). Theory and application for the scanning tunneling microscope. *Physical Review Letters*, *50*, 1999–2001.

Xi, Y., Ishikawa, H., Bin, Y., & Matsuo, M. (2004). Positive temperature coefficient effect of LMWPE-UHMWPE blends filled with short carbon fiber. *Carbon*, *42*, 1699–1706.

Zhang, R., Bin, Y., Dong, E., & Matsuo, M. (2014). Considerable different frequency dependence of dynamic tensile modulus between self-heating (Joule heat) and external heating for polymer-nickel coated carbon fiber composites. *Journal of Physical Chemistry B*, *118*, 7047–7058.

Zhang, P., Bin, Y., Zhang, R., & Matsuo, M. (2014). Joule heat of dynamic tensile modulus of polyimide-vapor grown carbon fiber nanocomposites under applied electric field evaluated in terms of thermal fluctuation-induced tunneling effect. *Polymer*, *55*, 2597–2608.

Zhang, P., Bin, Y., Zhang, R., & Matsuo, M. (2017). Average gap distance between adjacent conductive fillers in polyimide matrix calculated using impedance extrapolated to zero frequency in terms of a thermal fluctuation-induced tunneling effect. *Polymer Journal*, *49*, 839–850.

Zhu, D., Zhang, J., Bin, Y., Gin, C., Shen, J., & Matsuo, M. (2012). Dielectric studies on the heterogeneity and interfacial property of composite mode of polyacene quinine radical polymers and sulfonated polyurethanes. *Journal of Physical Chemistry A*, *116*(9), 2024–2031.

Supplementary Material: The online version of this article offers supplementary material (https://doi.org/10.1515/cti-2020-0014).